Differential cleavage of lysyl oxidase by the metalloproteinases BMP1 and ADAMTS2/14 regulates collagen binding through a tyrosine sulfate domain

Received for publication, January 29, 2019, and in revised form, May 24, 2019 Published, Papers in Press, May 31, 2019, DOI 10.1074/jbc.RA119.007806

Tamara Rosell-García[‡], Alberto Paradela[§], Gema Bravo[§], Laura Dupont[¶1], Mourad Bekhouche[¶], Alain Colige[¶2,3], and Fernando Rodriguez-Pascual[‡3,4]

From the [‡]Centro de Biología Molecular "Severo Ochoa," Consejo Superior de Investigaciones Científicas (C.S.I.C.), Universidad Autónoma de Madrid, E-28049 Madrid, Spain, the [§]Proteomics Facility, Centro Nacional de Biotecnología, Consejo Superior de Investigaciones Científicas (C.S.I.C.), E-28049 Madrid, Spain, and the [¶]Laboratory of Connective Tissues Biology, GIGA, University of Liège, 4000 Sart Tilman, Belgium

Edited by Gerald W. Hart

Collagens are the main structural component of the extracellular matrix and provide biomechanical properties to connective tissues. A critical step in collagen fibril formation is the proteolytic removal of N- and C-terminal propeptides from procollagens by metalloproteinases of the ADAMTS (a disintegrin and metalloproteinase with thrombospondin motifs) and BMP1 (bone morphogenetic protein 1)/Tolloid-like families, respectively. BMP1 also cleaves and activates the lysyl oxidase (LOX) precursor, the enzyme catalyzing the initial step in the formation of covalent collagen cross-links, an essential process for fibril stabilization. In this study, using murine skin fibroblasts and HEK293 cells, along with immunoprecipitation, LOX enzymatic activity, solid-phase binding assays, and proteomics analyses, we report that the LOX precursor is proteolytically processed by the procollagen N-proteinases ADAMTS2 and ADAMTS14 between Asp-218 and Tyr-219, 50 amino acids downstream of the BMP1 cleavage site. We noted that the LOX sequence between the BMP1- and ADAMTS-processing sites contains several conserved tyrosine residues, of which some are post-translationally modified by tyrosine *O*-sulfation and contribute to binding to collagen. Taken together, these findings unravel an additional level of regulation in the formation of collagen fibrils. They point to a mechanism that controls the binding of LOX to collagen and is based on differential BMP1- and ADAMTS2/14-mediated cleavage of a tyrosine-sulfated domain.

The extracellular matrix (ECM)[5] is a complex scaffold resulting from the association of diverse macromolecules produced and secreted by cells into the surrounding medium. This ECM not only provides structural support for resident cells but also influences various cellular processes, including proliferation, adhesion, migration, and differentiation, as well as plays key roles in homeostasis and the regeneration of tissues and organs (1). Although the composition of the ECM can vary markedly, collagens are the main component conforming the structural matrix core and are fundamental to providing the connective tissues with their biomechanical properties. In vertebrates, 28 types of collagens have been described (I–XXVIII), which are classified into several families, including the fibrillar collagen family (I–III, V, XI, XXIV, and XXVII) and basement membrane-forming collagen IV (2). Fibrillar collagens form homotrimeric (three identical α-chains) or heterotrimeric (two or three distinct polypeptide chains) molecules. Each α-chain consists of a major uninterrupted triple helical or collagenous domain (characterized by a repetition of Gly-Xaa-Yaa triplets, where Xaa and Yaa are commonly proline and hydroxyproline, respectively) flanked by N- and C-terminal noncollagenous domains, the N- and C-propeptides (3). Once synthesized in the endoplasmic reticulum, these collagen chains are brought together in a process governed by the C-propeptides and folded to form the procollagen molecule. Upon transit through the Golgi network and extracellular secretion, the N- and C-propeptides are cleaved off, respectively, by the procollagen N-proteinases belonging to the ADAMTS (a disintegrin and metalloproteinase with thrombospondin motifs) family (ADAMTS2, -3, and -14) and by C-proteinases, which are BMP1 (bone morphogenetic protein 1)/Tolloid-like enzymes. These proteolytic events yield triple helical collagen molecules that retain only a short portion of the propeptides, the telopeptides, and are able to assemble into fibrils, the most recognizable signature of collagen-based extracellular structures (3).

This work was supported in part by Grants from Ministerio de Economía y Competitividad, Plan Nacional de I+D+I: Grants SAF2012-34916 and SAF2015-65679-R (to F. R.-P.), "Fonds Léon Frédericq" FRSM, T.0183.13, and a grant from the "Anti-cancéreux." F. R.-P. reports grants from Pharmaxis, outside the submitted work.

This article contains Figs. S1–S5.

[1] Supported by a "Télévie" grant.

[2] Senior Research Associate of the FRS-FNRS.

[3] Both authors contributed equally to this work.

[4] To whom correspondence should be addressed: Centro de Biología Molecular "Severo Ochoa," Consejo Superior de Investigaciones Científicas (C.S.I.C.), Universidad Autónoma de Madrid (U.A.M.), Nicolás Cabrera, 1 E-28049 Madrid, Spain. Tel.: 34-91-196-4505; Fax: 34-91-196-4420; E-mail: frodriguez@cbm.csic.es.

[5] The abbreviations used are: ECM, extracellular matrix; LOX, lysyl oxidase; PTM, post-translational modification; Dox, doxycycline; FBS, fetal bovine serum; ADAMTS, a disintegrin and metalloproteinase with thrombospondin motif; LOXL, lysyl oxidase-like; PRM, parallel reaction monitoring; BAPN, β-aminopropionitrile; ANOVA, analysis of variance; HRP, horseradish peroxidase; Tet, tetracycline; TR, tetracycline repressor.

The mechanical strength of the extracellular collagenous matrix is highly dependent on the formation of covalent cross-links within fibrils, a process initiated by the enzymatic action of lysyl oxidase (LOX) (4). LOX catalyzes the oxidative deamination of lysine and hydroxylysine residues within the telopeptide domains, yielding the corresponding aldehydes, which eventually condense with other oxidized groups or intact lysines to form a variety of inter- and intrachain cross-linkages. Five different LOX enzymes have been identified in mammals (LOX and LOX-like 1–4), with the canonical LOX being the isoform most clearly associated with the remodeling and stability of the collagen matrix, described to play important roles in fibrosis, tumor microenvironment, and tissue repair (5, 6).

Proteolysis is crucial in the process of collagen synthesis and assembly. Not only are proteolytic events responsible for the removal of the propeptides, but also one of involved proteases, namely BMP1, cleaves the LOX precursor to generate the propeptide, for which biological activities have been also reported, and the fully active LOX (7–10). This simple picture is, however, challenged by experimental evidence showing that different mature forms co-exist and contribute to LOX-mediated actions (11–14). The molecular mechanisms leading to this behavior, which may arise not only by alternative proteolytic processing but also because of post-translational modifications (PTM), have not been established, and its study might indeed shed fresh light on the biological function of LOX. In this context, we recently identified, using a large-scale and nonbiased approach, that LOX is a potential substrate of ADAMTS14, although a complete characterization of this potential proteolysis remains to be investigated, as well as its relevance in the regulation of LOX (15).

Here, we describe that LOX is proteolytically processed by ADAMTS2 and -14, but not ADAMTS3, between residues Asp-218 and Tyr-219, at a site located 50 amino acids downstream of the well-characterized BMP1 cleavage site. Protein segment flanked by both processing sites contains a number of conserved tyrosine residues that can be potentially modified by tyrosine *O*-sulfation, which we confirmed by different methodological approaches, including proteomic characterization. Although we have shown that the LOX precursor and the forms processed by BMP1 or ADAMTS2/14 proteases displayed similar enzymatic activity on a soluble substrate, they substantially differed in their capacity to bind collagen, with the sulfotyrosine residues playing an important role in the interaction. Taken together, these results point to a mechanism for the regulation of the binding and the activity of LOX on collagen, resulting from the differential cleavage by BMP1 and ADAMTS2/14 of a tyrosine sulfate domain.

Results

LOX is expressed in multiple forms

By using a polyclonal antibody that specifically recognizes the C-terminal end of LOX protein, we have analyzed the electrophoretic pattern of LOX secreted from human lung fibroblasts and bovine endothelial cells incubated for 4 days in the presence or absence of the cytokine transforming growth factor-β1 (TGF-β1), a well-known activator of LOX expression

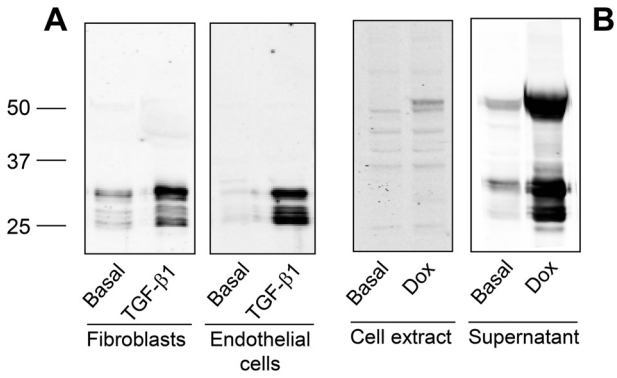

Figure 1. LOX isoform is expressed in multiple forms. *A,* human lung fibroblasts and bovine vascular endothelial cells were incubated for 4 days under basal conditions or in the presence of 5 ng/ml TGF-β1. Then, cell supernatants were taken and concentrated using a 10-kDa cutoff centrifugal filter. An aliquot was fractioned by SDS-PAGE and assayed by immunoblotting with a specific LOX antibody recognizing the C-terminal catalytic domain. Multiple immunoreactive bands were observed with molecular masses ranging from 25 to 30 kDa. *B,* generation of HEK293 cells overexpressing human LOX in a tetracycline inducible manner. LOX protein in the total cell extract and in the supernatant was assessed by immunoblotting under basal conditions and upon induction with the tetracycline analog, Dox. The precursor form at 50 kDa and multiple shorter forms (at 25–30 kDa) are identified in the culture medium of Dox-treated cells. The blots shown correspond to representative experiments performed twice with two independent preparations.

(16). As shown in Fig. 1*A*, the supernatant of fibroblasts or endothelial cells showed multiple immunoreactive bands ranging from 25 to 30 kDa, whose levels strongly increased upon incubation with TGF-β1. To analyze how this pattern arises, we have generated a human embryonic kidney (HEK) 293 cell clone stably expressing a human LOX construct under tetracycline-dependent control. Fig. 1*B* shows the LOX immunoreactivity associated with cells (cell extract) or secreted into the extracellular medium (supernatant) in basal conditions or upon stimulation with doxycycline, a tetracycline analog. Although only a very faint band of about 50 kDa, corresponding to the intracellular precursor, was observed in the extracts from stimulated cells, significantly higher levels were secreted to the extracellular medium, including the precursor and multiple bands at 25–30 kDa. In contrast to fibroblast and endothelial cultures, where precursor bands were not detected under our experimental conditions, HEK293 cell clone displayed a limited capacity to process LOX as indicated by the accumulation of the unprocessed form, a circumstance providing the possibility to use this cell line to analyze the molecular events associated to the generation of mature forms.

ADAMTS2 and -14 proteolytically process LOX

We have previously identified LOX as a potential substrate of ADAMTS14 in the secretome of human fibroblasts (15). Here, we used two methodological approaches to characterize the ability of the procollagen N-proteinases, ADAMTS2, -3, and -14, to cleave LOX. Having generated HEK293 cell clones stably expressing the human forms of these ADAMTS proteases only in the presence of doxycycline (Fig. S1), we co-cultured them with HEK293 cells able to conditionally secrete LOX. After 48 h of co-culture with or without doxycycline, the LOX pattern was evaluated by immunoblotting (Fig. 2, *A* and *B*). Expression of ADAMTS2 and ADAMTS14 resulted in a relative enrichment

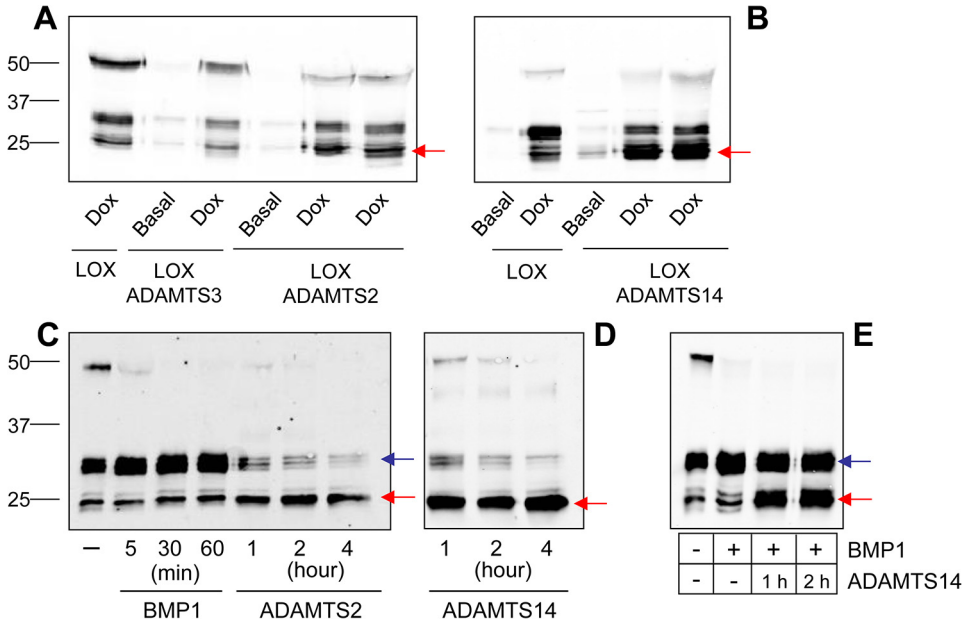

Figure 2. Cleavage of LOX by ADAMTS2 and ADAMTS14. LOX cleavage was assayed by immunoblotting in LOX/ADAMTS-overexpressing co-cultures after incubation with doxycycline for 48 h (*A* and *B*) and after *in vitro* incubation assays (*C* and *D*) for the indicated times. For comparison, LOX fragments generated upon incubation with BMP1 are also shown in *C*. ADAMTS2 and ADAMTS14, either in co-culture or using purified proteins, promoted the accumulation of a mature form of about 25 kDa (*red arrow*), whereas BMP1 cleavage gave rise to bands in the 30-kDa range (*blue arrow*), indicating distinct processing sites. ADAMTS3 co-culture did not modify the relative levels of both fragments, suggesting it was not able to process LOX under our experimental conditions. *E*, sequential incubation with BMP1 and ADAMTS14. LOX supernatant was first incubated with BMP1 for 1 h. Then, ADAMTS14 was added into the reaction mixture for the indicated times.

of mature forms of LOX around 25 kDa, at the expense of bands at 30 kDa, strongly suggesting a proteolytic processing. Such cleavage was not observed for ADAMTS3. It has to be mentioned that HEK293 cells display significant endogenous BMP1, which explains the conversion of precursor LOX into forms migrating around 30 kDa. We have also established an *in vitro* assay for the analysis of LOX cleavage by incubation of concentrated supernatants from LOX-overexpressing clone and purified preparations of ADAMTS2 and ADAMTS14, and we compared their effects with that of concentrated supernatants from HEK293 cells overexpressing BMP1 (Fig. S1 and Fig. 2, *C* and *D*). Similar to data obtained in co-cultures, incubation with ADAMTS2 and ADAMTS14 resulted in a time-dependent reduction of the abundance of the 50-kDa LOX precursor and a concomitant accumulation of the mature form at 25 kDa. In contrast, incubation with BMP1 led to an enrichment of the processed forms around 30 kDa, clearly indicating that ADAMTS enzymes process LOX in a different location, presumably downstream from the established BMP1 site. This aspect was further confirmed by complete proteolysis by BMP1 and addition of ADAMTS14 on top of the BMP1-processed form (Fig. 2*E*).

We then applied a proteomic approach to determine at which site LOX is cleaved by ADAMTS2/14. For that purpose, LOX supernatants exposed to ADAMTS2 were filtered through a 50-kDa-cutoff centrifugal filter to enrich the samples in LOX mature forms (Fig. S2). Flow-throughs were trypsin-digested, and peptides were analyzed by MS (Fig. 3). Several LOX peptides were identified that resulted from trypsin digestion at both their N- and C-terminal ends, except one hemityptic (a peptide cleaved by trypsin in one end and another protease in the other end), *i.e.* cleaved by trypsin at the C terminus but not at the N terminus, presumably obtained by ADAMTS2-dependent action. In fact, careful inspection of this potential processing site within the LOX sequence revealed its location 50 residues downstream of the well-established BMP1 site, an observation that fully matches with the molecular weight of the ADAMTS2/14-processed form as observed by immunoblotting. Analysis of LOX protein sequence shows that both BMP1 (MVG/DDP) and ADAMTS (VAD/PYY) sites are well-conserved among several organisms (Fig. 4). Interestingly, the Asp/Pro scissile bond cleaved by ADAMTS2 and -14 is also conserved in LOX forms evolutionarily close to the canonical LOX, such as lysyl oxidase-like (LOXL) isoform 1 or the zebrafish LOXL5 (a sort of hybrid LOX/LOXL1 uniquely present in this teleost fish). By contrast, the more evolutionarily distant LOXL2, LOXL3, and LOXL4 isoforms display no homology in the corresponding position, despite the overall conservation observed in the downstream catalytic domain (5). This observation predicts that LOXL1 and LOXL5 proteins might be also substrates of ADAMTS proteases.

To evaluate LOX cleavage by ADAMTS2 and ADAMTS14 in a relevant cell model, we used skin fibroblasts isolated from wildtype (WT) and *Adamts2–Adamts14*-deficient mice (17). These fibroblasts were left untreated or were incubated with TGF-β1 (5 ng/ml during 48 h). Conditioned media were then analyzed by immunoblotting. As shown in Fig. 5, for WT fibroblasts incubated with TGF-β1, the vast majority of the LOX signal was detected around 25 kDa, which corresponds to the ADAMTS2/14 processed forms. By contrast, upon induction with TGF-β1, fibroblasts from the double knockout showed a diminishing of the 25-kDa product with respect to WT, without significantly affecting the BMP1 product at 30 kDa, which dem-

A

MRFAWTVLLL GPLQLCALVH CAPPAAGQQQ PPREPPAAPG AWRQQIQWEN NGQVFSLLSL
GSQYQPQRRR DPGAAVPGAA NASAQQPR**TP** **ILLIR**DNRTA AARTRTAGSS GVTAGRPRPT
ARHWFQAGYS TSRAREAGAS RAENQTAPGE VPALSNLRPP SR**VDGMVGDD** **PYNPYK**YSDD
NPYYNYYDTY ERPRPGGRYR PGYGTGYFQY GLPDLVAD**PY YIQASTYVQK** **MSMYNLRCAA**
EENCLASTAY **R**ADVRDYDHR VLLRFPQR**VK** **NQGTSDFLPS** **RPR**YSWEWHS CHQHYHSMDE
FSHYDLLDAN TQRRVAEGHK **ASFCLEDTSC** **DYGYHR**RFAC TAHTQGLSPG CYDTYGADID
CQWIDITDVK **PGNYILK**VSV NPSYLVPESD YTNNVVRCDI R**YTGHHAYAS** **GCTISPY**

B

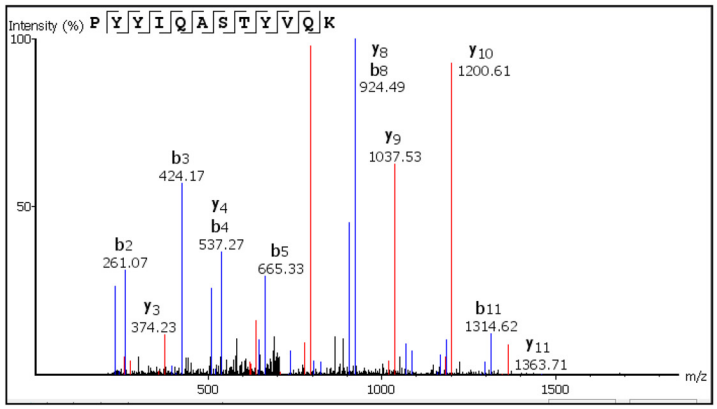

C

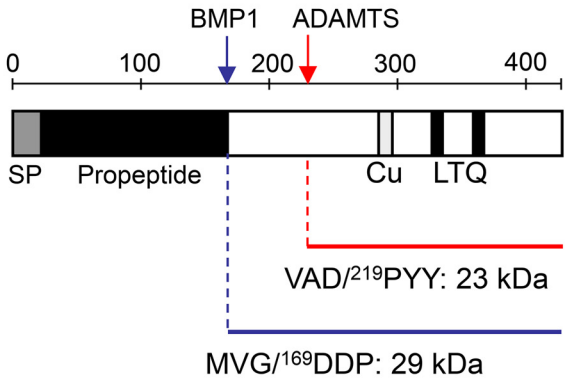

Figure 3. Proteomic characterization of the ADAMTS-mediated cleavage site in LOX protein. LOX supernatants exposed to ADAMTS2 were enriched in LOX mature forms by passing through a 50-kDa cutoff centrifugal filter. Then, the flow-throughs were trypsin-digested, and the resulting peptides were fractionated by LC and analyzed by MS. *A,* peptide coverage along the human LOX sequence showing identified tryptic fragments (shown in *bold*) as well-as a hemitryptic peptide that resulted from the action of ADAMTS2 (*yellow,* fragment ion spectra in *B*). *C,* schematic representation of the cleavage site by BMP1 (*blue arrow* and *arrowhead* in *A*) and ADAMTS2/14 (*red arrow* and *arrowhead* in *A*) within LOX. The cleaved sequences and the theoretical molecular weights of the LOX forms generated by these cleavages are also provided.

onstrates the participation of ADAMTS2/14 in the maturation of LOX.

Identification of tyrosine sulfation in the region of LOX protein flanked by BMP1 and ADAMTS2/14 processing sites

Examination of the LOX immunoreactive bands throughout this study showed that they are actually formed by multiple molecular species differing slightly in their electrophoretic mobility, a behavior typically arising from extensive PTM. We have investigated this possibility by two-dimensional (2D) electrophoresis followed by immunoblotting. As shown in Fig. 6, precursor and mature forms of LOX are visualized as several spots. Interestingly, LOX precursor at 50 kDa, with a theoretical isoelectric point (pI) of 7.99, gave rise to a train of spots at a much more acidic pI, an observation indicating the presence of PTM added extra negative charges (Fig. 6*A*). Upon cleavage with the BMP1 enzyme, the most acidic part of this series of spots is kept, whereas the digestion with ADAMTS2 collapsed these species into a single spot at a more basic pI (Fig. 6, *B* and *C*). These observations are compatible with the findings that the presence of the PTM caused the acidic shift within the protein region flanked by BMP1 and ADAMTS sites. This region, depicted in Fig. 7*A*, represents a unique tract within LOX sequence as it contains 12 tyrosines in a 50-amino acid–long segment, most of them well-conserved among different LOX orthologs (see Fig. 4). Tyrosine *O*-sulfation is one of the PTMs known to add extra negative charges and has been increasingly recognized as an important regulator of protein–protein interactions in the extracellular space (18, 19). In fact, tyrosine sulfation of LOX in this particular location has been previously suggested but, to our knowledge, not thoroughly investigated (20). Analysis of LOX sequence using Sulfinator, a software used to predict tyrosine sulfation sites, revealed candidate tyrosines for this modification in a cluster within this region (Fig. 7*A*) (21). As a first approach to investigate whether these tyrosine residues become sulfated, we have altered the LOX sequence by changing tyrosines into phenylalanines, which blocked sulfation, and analyzed the mutant protein by immunoblotting under control conditions and after processing with BMP1 and ADAMTS enzymes. As shown in Fig. 7*B* (*left*), the precursor of this LOX mutant in the tyrosine cluster showed a slightly increased electrophoretic mobility compared with the WT precursor, an effect much more evident in the forms processed by BMP1. In contrast, the products resulting from ADAMTS2 cleavage migrated similarly for both WT and mutant proteins. Altogether, these observations suggest that these tyrosine residues are the target of a particular chemical modification, and its mutation abolishes this effect. This interpretation is further supported by 2D electrophoresis showing that LOX spots corresponding to the precursor band and the BMP1-processed form were shifted to the right in the mutant, whereas both WT and mutant forms accumulated into the same spot after proteolysis with ADAMTS2 (Fig. S3). Evidence

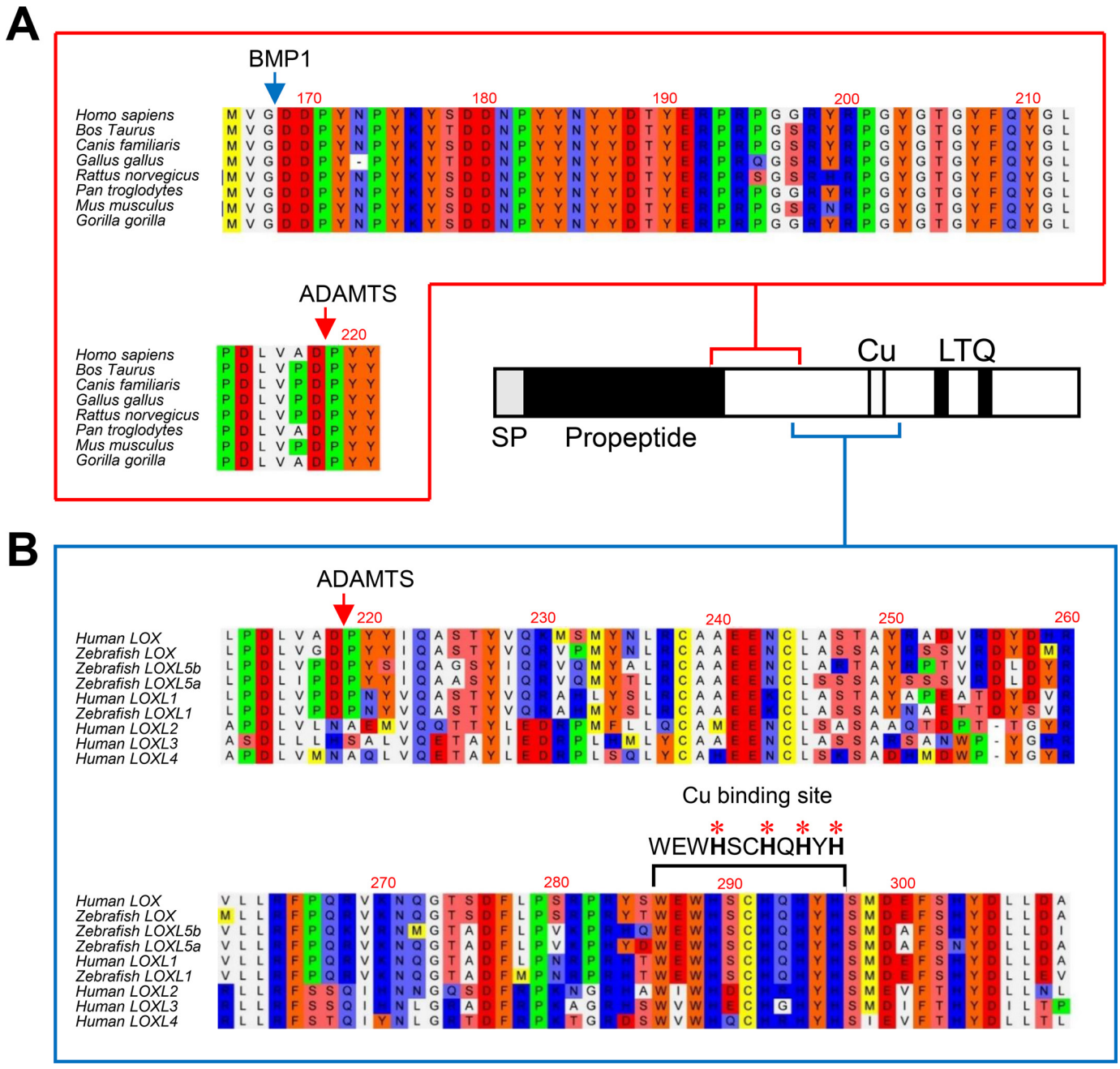

Figure 4. Multiple sequence alignments of ADAMTS cleavage site and flanking sequences. *A,* sequence alignment of LOX orthologs from the indicated species showing high homology at the ADAMTS and BMP1 cleavage sites and also in between. *B,* sequence alignment of ADAMTS cleavage site and downstream sequences from LOX orthologs and paralogs from the indicated species. Of note is the high degree of homology observed between the cleavage site characterized in human LOX and corresponding sequences of human LOXL1 and the zebrafish LOX, LOXL1, and LOXL5 isoforms. On the contrary, no significant homology was found among LOXL2, LOXL3, and LOXL4 paralogs, despite the conservation observed in the downstream histidine-rich catalytic core. Protein alignments were done with the ClustalW2 program (http//www.ebi.ac.uk; please note that the JBC is not responsible for the long-term archiving and maintenance of this site or any other third party hosted site.

for a sulfotyrosine modification was additionally obtained by using an antibody recognizing this particular PTM. As shown in Fig. 7*B* (*right*), this antibody positively stained the form processed by BMP1 in the WT but not in the mutant protein, leaving unstained the ADAMTS2-processed forms. Because our antibodies are not efficient for immunoprecipitation, we then generated LOX fused to green fluorescent protein (GFP). First, as shown in Fig. 7*C*, we confirmed that LOX–GFP chimeras behaved essentially as the corresponding forms without the GFP-tag, *i.e.* both forms are substrates for BMP1 and ADAMTS2 proteases, and tyrosine residues are the subject of a PTM modifying the electrophoretic mobility of precursor and the BMP1-processed forms. Then, these cell clones were metabolically labeled with inorganic [^{35}S]sulfate, and the labeling of LOX proteins was determined after immunoprecipitation by electrophoresis and autoradiography. As shown in Fig. 7*D* (*left*), sulfated polypeptides corresponding to BMP1-processed forms were identified for the WT LOX–GFP, whereas no labeling of the ADAMTS2-cleaved product was observed. Despite the proven ability of the anti-GFP beads to

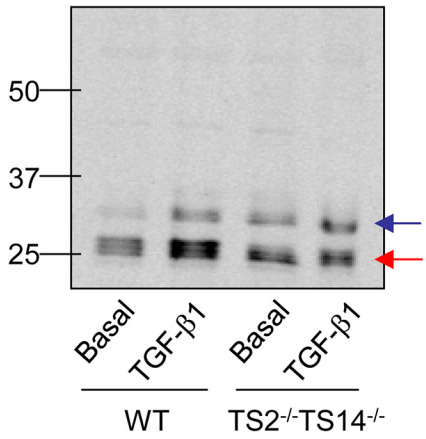

Figure 5. LOX cleavage in skin fibroblasts from WT and *Adamts2–Adamts14*-deficient mice. Accumulation of LOX mature forms in the extracellular medium was assayed by immunoblotting in cultured skin fibroblasts from wildtype (*WT*) and doubly-deficient *Adamts2–Adamts14* knockout mice (*TS2*$^{-/-}$*TS14*$^{-/-}$) upon induction with TGF-β1 or basal. Note that ADAMTS2/TS14-deficient cells showed a diminishing of the 25-kDa product (*red arrow*) with respect to WT, without significantly affecting the 30-kDa BMP1 product (*blue band*) (ratio of band intensities ADAMTS/BMP1:3.71 in the WT; 1.45 in *Adamts2-Adamts14*-deficient fibroblasts).

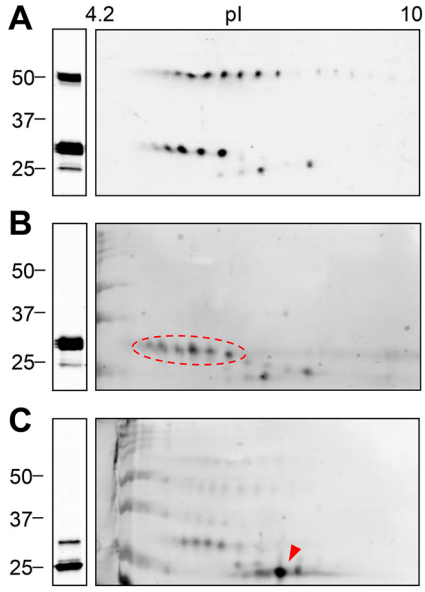

Figure 6. Analysis of LOX proteolysis by two-dimensional electrophoresis coupled to immunoblotting. LOX supernatants kept under basal conditions (*A*) or incubated with BMP1 (*B*) or ADAMTS2 (*C*) were fractioned by 1D (*left*) or 2D (*right*) electrophoresis and analyzed by immunoblotting using a specific C-terminal LOX antibody. LOX precursor was visualized as a train of spots with the isoelectric point (pI) more acidic than predicted from the amino acid sequence (7.99). BMP1-cleaved mature form gave a similar pattern (indicated by a *red dashed oval*), whereas the cleavage by ADAMTS2 resulted in a single prominent spot at a more basic pI (*red arrowhead*). The blots shown correspond to representative experiments performed twice with two independent preparations.

pull down the LOX proteolytic fragments in the LOX–GFP mutant protein (Fig. 7*D*, *right*), no radioactive-labeled bands were detected for this chimera. Finally, we have also performed a proteomic characterization of immunoprecipitated LOX–GFP bands resulting from proteolysis with BMP1 by parallel-reaction monitoring (PRM). Because of restrictions imposed by sequence, instead of performing a conventional digestion with trypsin, we processed protein bands with AspN, and therefore, we could only analyze the peptide DDNPYYNYY (Figs. S4 and S5). By comparison with synthetic peptides harboring sulfotyrosines at different positions, we were able to unambiguously detect the sulfuryl moiety in the last tyrosine residue of this peptide (Tyr-187), and also in one of the previous doublet, with no distinction of the exact position (Tyr-183 or Tyr-184). Disulfotyrosine peptides were not detected, most likely because negatively charge residues cannot stay in close proximity.

Taken together, these results demonstrate that tyrosine residues in the LOX sequence flanked by cleavage sites for BMP1 and ADAMTS2/14 undergo sulfation, a modification that potentially can influence the biological properties of the LOX enzyme.

Biological effect of the proteolytic processing of LOX: contribution of the tyrosine-sulfated domain for binding to collagen

Having demonstrated that LOX is processed by ADAMTS2/14, we investigated the contribution of this cleavage to the enzymatic activity while comparing with the effect of BMP1. LOX enzymatic activity was determined in an *in vitro* assay using a soluble substrate through detection of peroxide in a horseradish peroxidase (HRP)-coupled real-time reaction (22). Using this method, we observed that supernatants from doxycycline-induced HEK293 cells displayed strong increases in LOX activity compared with supernatants from cells left under basal conditions, which is clearly attributed to the induction of the expression of LOX protein (Fig. 8*A*). The presence of β-aminopropionitrile (BAPN, LOX inhibitor) resulted in a complete inhibition of this induction, which further demonstrated the specificity and relevance of the assay (Fig. 8, *A* and *B*). As also shown in Fig. 8, incubation of LOX with ADAMTS2 did not significantly modify its activity. To our surprise, treatment with BMP1, the well-established activator of LOX, left the activity essentially unchanged. Therefore, in contrast to previous assumptions, these observations suggest that the precursor is catalytically active and that the processing by BMP1 or ADAMTS enzymes does not substantially enhance this intrinsic enzymatic activity. In addition to elastin and collagen substrates, LOX enzyme can also oxidize a variety of mono- or diamines of various carbon chain lengths (23, 24). Given the apparent flexibility of substrate requirements, which has permitted the development of a convenient (and widely used) HRP-coupled assay, our observations suggest that, rather than the enzymatic capacity of the LOX protein, proteolysis may determine the interaction with substrates, and thereby restrict its activity *in vivo* on collagen and elastin (22). We have therefore investigated the capacity of the precursor and processed forms of WT and tyrosine-mutated LOX to bind collagen in a modified solid-phase binding assay. HEK293-derived secretomes used in our studies do not contain pure LOX species, but rather a mixture resulting from the action of endogenous proteases, a confounding variable that can potentially give erroneous values in a standard colorimetric assay. For this reason, LOX-containing supernatants were incubated with immobilized collagens, either bearing telopeptides (telocollagen) or not (atelocollagen). Bound material was then collected and analyzed by SDS-PAGE coupled to immunoblotting. Using this

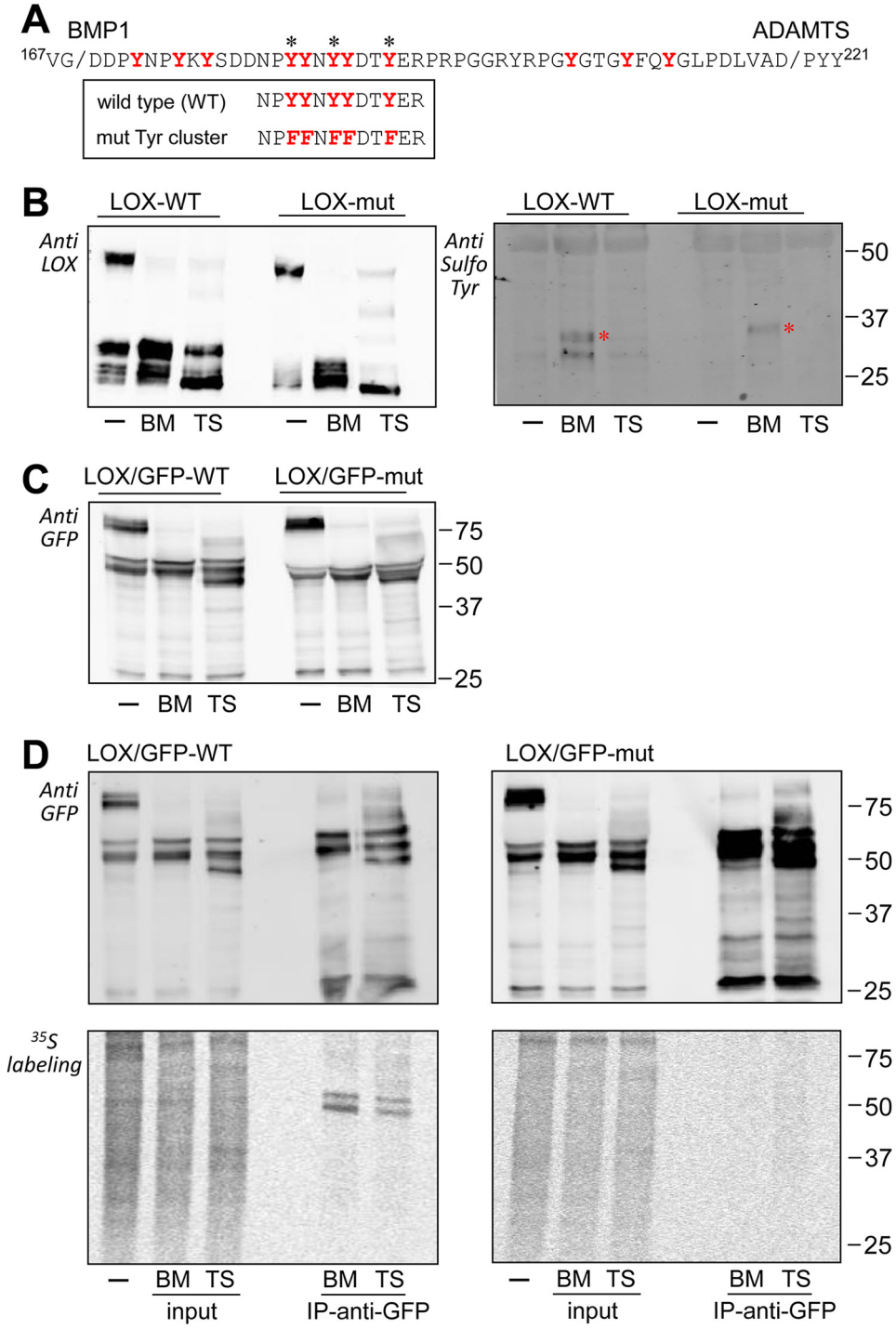

Figure 7. Identification of tyrosine sulfation in the LOX protein sequence flanked by BMP1 and ADAMTS2 cleavage sites. *A,* LOX protein sequence flanked by BMP1 and ADAMTS cleavage sites. Tyrosine residues conserved among LOX/LOXL1 orthologs are marked in *red*. *Asterisks* indicate tyrosines that are predicted to undergo sulfation by the algorithm Sulfinator. The sequences of the WT and mutant construct with the cluster of tyrosines changed to phenylalanine are also shown. *B,* cleavage of WT and mutant LOX by BMP1 (*BM*) and ADAMTS2 (*TS*) as assessed by immunoblotting with anti-LOX (*left*) and anti-sulfotyrosine (*right*) antibodies. The *asterisk* indicates the position of an unspecific band recognized by the antibody in both WT and mutant samples treated with BMP1. *C,* BMP1- and ADAMTS2-mediated cleavage of WT and mutant LOX chimera C-terminally fused to GFP as assessed by immunoblotting with an anti-GFP antibody. *D,* sulfation of tyrosines in LOX variants. HEK293 cells overexpressing WT (*left panels*) and mutant (*right panels*) LOX/GFP constructs were metabolically labeled with [^{35}S]sulfate. The supernatants were then kept untreated (−) or incubated with BMP1 or ADAMTS2 before immunoprecipitation (*IP*) using anti-GFP beads. Inputs and immunoprecipitates were analyzed by immunoblotting with an anti-GFP antibody (*upper panels*) and by autoradiography (*lower panels*). Note that only slow-migrating bands resulting from the action of BMP1 were shown to incorporate radioactivity, whereas the fragment with higher electrophoretic mobility specifically generated by ADAMTS2 was not. Radioactively labeled bands observed in the supernatant treated with ADAMTS2 likely represent fragments generated as a result of endogenous BMP1 secreted by HEK293 cells. No specific radioactive labeling was detected in the immunoprecipitates from mutant LOX/GFP.

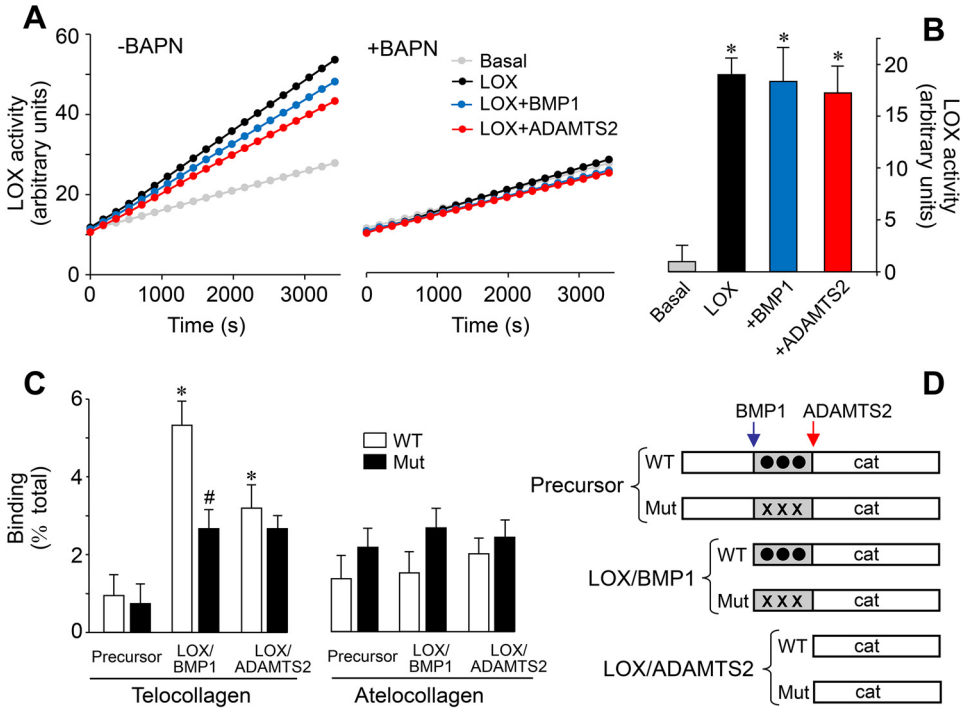

Figure 8. Effect of the proteolysis of LOX on enzymatic activity and collagen-binding capacity. Supernatants from LOX-overexpressing cells under control conditions (LOX) or exposed to BMP1 or ADAMTS2 were assessed for LOX enzymatic activity in a time-lapse fluorescence assay performed in the absence (*left panel*) or presence (*right panel*) of the LOX inhibitor BAPN (0.3 mM). Basal tracing represents the activity from a supernatant of a culture in the absence of induction with doxycycline. Representative data (*A*) and quantification from three independent experiments (*B*) are shown. Values are shown as fluorescent arbitrary units (mean ± S.D., $n = 6$, *, $p < 0.05$ *versus* basal). *C*, solid-phase binding assay to telocollagen (with intact telopeptides) or atelocollagen (without telopeptides) of the various LOX species shown in *D*. Binding capacity is shown as percentage of total (mean ± S.D., $n = 6$, *, $p < 0.05$ *versus* the corresponding control without protease treatment, #, $p < 0.05$ *versus* the corresponding WT). Statistical comparisons between groups were calculated by one-way ANOVA analysis followed by Bonferroni's post test.

approach, we could precisely determine the percentage of binding of the various LOX species (Fig. 8). The LOX precursor showed a limited capacity to bind telocollagen, and this was not modified by mutation of the tyrosine-sulfated domain. In contrast, BMP1-processed WT LOX displayed a higher binding capacity, a property that was markedly reduced for the tyrosine-mutated LOX, indicating that a substantial part of the interaction goes through these modified residues. Interestingly, the form processed by ADAMTS2 showed lower binding, and this was not altered in the mutant. Binding of LOX forms to atelocollagen was low and remained essentially unchanged upon proteolysis or mutation of tyrosine residues. Taken together, these results suggest that the differential cleavage of a tyrosine-sulfated domain by BMP1 and ADAMTS2/14 determines the capacity of an active LOX catalytic domain to interact with collagen and thereby direct it toward specific lysine residues in the telopeptide domain.

Discussion

The biosynthesis of collagen is a highly complex process involving numerous events occurring intra- and extracellularly (3). The final step, fundamental for providing the collagen network with its biomechanical properties, is the introduction of covalent cross-links, a process initiated by the enzymatic action of LOX (4). Current knowledge of the biological properties and functions of LOX is based upon *in vitro* investigations, mostly done during early works on matrix biology over the past century, and more recently generated *in vivo* knockout models (25). Based on this experimentation, it has been shown that LOX protein is secreted as an inactive precursor that is cleaved by BMP1 to yield the mature form responsible for the cross-linking of fibrillar collagens and elastin in the extracellular matrix of different tissues, mainly the vasculature, skin, and lung (7–10, 26–28). This study adds new players to this picture and provides novel structural information about LOX that is crucial for its biological activity. Here, we demonstrate that ADAMTS2 and ADAMTS14, two enzymes initially known for their aminoprocollagen peptidase activity, process LOX protein in a position downstream of the well-characterized BMP1 cleavage site and that the sequence between these sites contains a cluster of sulfated tyrosines essential for efficient collagen binding. Taken together, these data are consistent with the observation of multiple bands reported in numerous studies (11–13). They show also that the differential cleavage of LOX by BMP1 and ADAMTS2/14 modifies its affinity toward collagen and most probably its capacity to oxidize lysine residues in the telopeptide (Fig. 9). Analysis of the enzymatic activity of the various LOX species revealed that BMP1- and ADAMTS-mediated proteolysis did not significantly modify the capacity of an otherwise active precursor to oxidize a soluble substrate. The intriguing observation that the LOX precursor exhibits full activity in this assay opposes the widely accepted assumption of an inactive form becoming active upon cleavage by BMP1 (7–10). However, to our knowledge, no single study in the literature has shown the cleavage of LOX by BMP1 and the effect

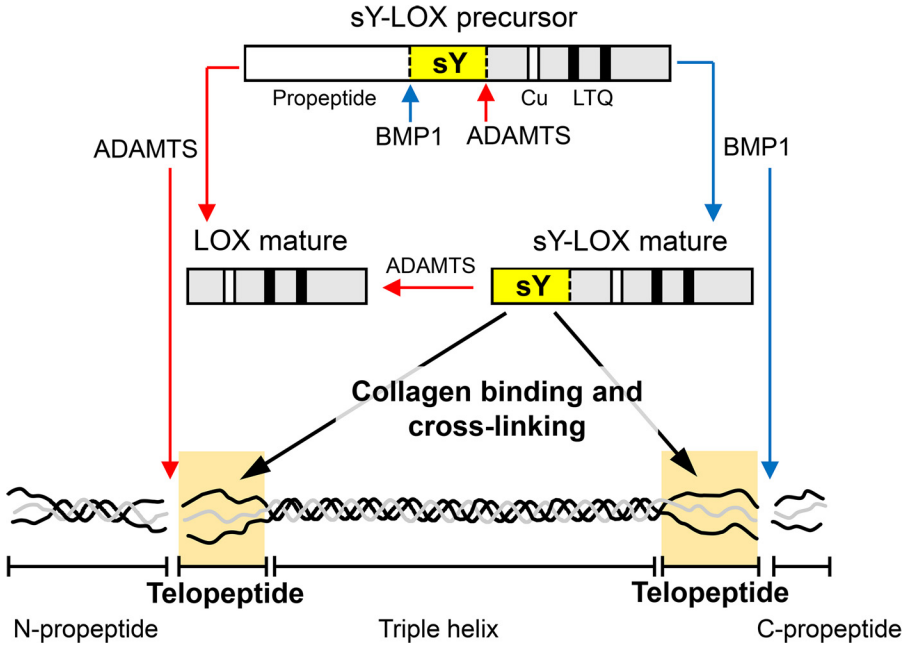

Figure 9. Schematic model describing LOX regulation by BMP1- and ADAMTS-mediated proteolysis in the context of collagen processing. The diagram summarizes the ability of these proteases to cleave LOX into two different locations yielding mature LOX species with different capabilities to bind collagen telopeptides based on the presence of a sulfotyrosine domain.

on its enzymatic activity *in vitro*, but rather indirect effects such as a reduced LOX activity in supernatants from protease-deficient cells, or enhanced LOX activity and processing, together with augmented insoluble collagen deposition in cells expressing higher levels of BMP1 mRNA (8, 29). In this respect, considering the flexibility of substrate requirements, with LOX capable of oxidizing not only collagen and elastin but also a variety of nonpeptidyl amines, we hypothesize that LOX activity is regulated by the extent of interaction with its different substrates, rather than by modification of its intrinsic enzymatic capacity (23, 24). Consistent with this hypothesis, we observed increased binding to immobilized collagen upon BMP1-mediated cleavage as compared with the unprocessed precursor. Previous studies have shown that the protein has a higher affinity, and thereby increased oxidation rate, on collagen present as fibrils, rather than in a soluble or denatured form (30, 31). Therefore, processing by BMP1 potentiates the capacity of LOX to interact with collagen fibrils, positioning the catalytically-active site close to the target lysines in the telopeptides. In fact, our experiments showed that LOX is capable of binding to both telo- and atelocollagen, with BMP1 action influencing specifically the capacity to interact with telopeptide-containing collagen. This is somewhat in contrast with previous studies showing that LOX exclusively interacts with the triple helical portion because the apparent binding affinity for native collagen was found to be quite similar to that for fibrils prepared from pepsin-digested collagen (30). However, it should be taken into account that these experiments were done with bovine aorta LOX preparations reported to be a mixture of multiple LOX species for which precise information about their individual binding features was not available (11).

An interesting observation of our results is the fact that cleavage by ADAMTS2 and -14 substantially diminished the capacity of LOX to bind telocollagen, indicating that an important part of the binding occurs through sequence determinants located between the BMP1 and ADAMTS cleavage sites. Using different methodological approaches, we demonstrate here that some tyrosine residues within this protein segment are modified by sulfation. Although our study could not make a complete characterization of the tyrosine residues present in this cluster, we succeeded in demonstrating sulfation of at least two different tyrosines. However, based on our 2D electrophoresis analyses, it can be anticipated that additional tyrosines outside this protein segment can also be modified. The importance of this PTM in the biological function of LOX is highlighted by the significant reduction in the collagen-binding capacity observed for the mutant construct. In fact, tyrosine sulfation has evolved as an important PTM mediating extracellular protein–protein interactions (18, 19). In the context of the extracellular matrix, several molecules, including fibromodulin, lumican, osteoadherin, and opticin, have been reported to contain clusters of sulfated tyrosine residues (32, 33). Particular attention to fibromodulin is needed as its tyrosine-sulfated domain has been reported to bind collagen and accelerate fibril formation (34). Molecular characterization of the binding properties of fibromodulin has revealed several areas of binding on the helical portion of type I collagen, with sulfotyrosines contributing to this interaction. Further mapping using triple-helical collagen toolkit peptides showed these sites partially overlap with the helical cross-linking sites (35). In fact, fibromodulin has turned out to be an important regulator of collagen cross-linking because its deficiency results in a dysregulated enhancement of collagen cross-links, which is associated with altered mechanical properties of tendinous tissues (36, 37). Interestingly, fibromodulin was also reported to bind LOX, and this interaction resulted in an apparent increase in LOX activity (35). Based on this information, a model of fibromodulin-regulated collagen cross-linking has been proposed where this small

leucine-rich protein, by forming a ternary complex at the helical cross-linking sites, directs LOX activity toward specific lysine residues on the telopeptide of an adjacent microfibril. Our results are in line with this hypothesis by endowing LOX protein with the capacity to interact directly with the telopeptides. Nevertheless, further experimentation is necessary to understand how the same PTM drives fibromodulin to the helical portion or makes LOX able to interact with the telopeptide ends, as well as whether tyrosine-sulfated domains are involved or not in the interaction between LOX and fibromodulin.

Proteolysis plays an important role in the homeostasis of connective tissues, not only by allowing the degradation of structural components but also by regulating the capacity of a large array of macromolecules to assemble into a well-organized physiological ECM. BMP1 and ADAMTS enzymes, responsible for the processing of procollagen and, as studied here, of the precursor of LOX protein, have been described to cleave a wide variety of substrates, most of them belonging to the ECM category. BMP1 and its related tolloid-like enzymes were reported to cleave small leucine-rich proteoglycans (biglycan and decorin), basement membrane components (such as laminin), and mineralization factors, including dentin sialoprotein and phosphophoryn (38). Additionally, recent work from our group has significantly expanded the substrate repertoire of ADAMTS procollagenases with the identification of fibronectin, some fibulins, thrombospondin-1, decorin, and perlecan, among many others (15). Altogether, these studies permitted us to establish preferential cleavage sites for these proteases. Processing by BMP1 seems to be quite restricted, with most substrates displaying an aspartate in the P1′ position (39). For ADAMTS procollagenases, however, although identified cleavage sites were found to be enriched in proline and glycine residues, a clear consensus sequence has not yet been well-defined (15). The LOX precursor fulfills the strict aspartate requirement for BMP1 proteolysis, and proline is well-represented within the well-conserved ADAMTS cleavage site in orthologs from different species (see Fig. 4). Given the critical role of these proteases in collagen biosynthesis, gene defects that alter their expression and/or activity are expected to cause disease. Recessive mutations in BMP1 are linked with recessive forms of osteogenesis imperfecta, a heterogeneous group of bone disorders characterized by fragile bones that break easily (40). The *ADAMTS2* gene is associated with the dermatosparaxis-type of Ehlers-Danlos syndrome, a rare condition characterized by extreme skin fragility (41–43). At the molecular level, both clinical conditions display defective procollagen processing, which is claimed to be responsible for the production of collagen molecules with altered structure leading to aberrant matrix in affected tissues. Collagen cross-linking is likely to be dysregulated in these connective tissue disorders. However, considering the overall matrix involvement and the fact that these proteases process other matrix components, this aspect has been poorly investigated. Rare variants in the *LOX* gene have been identified that disrupt enzyme function and promote thoracic aortic aneurysms because of insufficient elastin and collagen cross-linking in the aortic wall (44, 45). Sequence variations have been also found that fall within and around the BMP1 and ADAMTS cleavage sites, or even alter the tyrosine residues modified by sulfation (46). Their functional consequences have not yet been investigated. However, it can be speculated that they can alter the proteolytic activation of LOX or the binding characteristics of the sulfated domain. Further studies in patient or animal models will be required to gain insight into how BMP1, ADAMTS2, and ADAMTS14 coordinately regulate collagen processing and cross-linking, as well-as the contribution of these genetic variants to the process.

In conclusion, our data provide novel knowledge about the proteolytic regulation of LOX functions, linking the differential action of BMP1 and ADAMTS procollagenases on a sulfated tyrosine domain to the capacity of LOX to bind and oxidize collagen in the context of extracellular matrix synthesis and deposition.

Experimental procedures

Cell culture

Tetracycline (Tet)-inducible HEK293 cells stably expressing LOX, ADAMTS, and BMP1 constructs were generated and maintained in culture according to protocols published previously (15, 47). Human lung fibroblasts from the cell line CCD-19Lu were obtained from the American Type Culture Collection (Manassas, VA) and maintained in culture medium as already described (48). Primary bovine aortic endothelial cells were isolated from thoracic aortas and maintained in culture using previously described methods (49).

Skin fibroblast cultures from mice doubly-deficient for *Adamts2* and *Adamts14* were established as follows (17). After sacrifice, mice were shaved and a skin fragment from the belly of approximately 2 cm^2 was collected, washed in 70% ethanol, transferred in culture hood, rinsed in sterile PBS, and cut into 1-mm^2 pieces. Skin fragments were then incubated at 37 °C in 10 ml of complete Dulbecco's modified Eagle's growth medium supplemented with collagenase (Sigma) at 1000 units/ml. After 2 h, 10 ml of complete medium supplemented with 10% fetal bovine serum (FBS) was added, and centrifugation was performed (5 min at 500 × *g*). The pellet was homogenized by pipetting in 10 ml of warm complete medium containing 15% FBS, transferred into 10-cm tissue culture dishes, and placed into an incubator under hypoxic conditions (at 37 °C, 5% CO_2, 5% O_2). Fibroblasts expand from tissue fragments within 2–5 days and can be amplified (1:3 ratio) for up to 10 passages when kept in hypoxia.

Construction of LOX, ADAMTS, and BMP1 constructs and generation of stable clones for overexpression

A full-length human LOX construct in pYX-Asc vector was obtained from Imagenes GmbH (Berlin, Germany). A full-length human BMP1 construct in pBabe vector was kindly provided by Víctor L. Ruiz-Pérez (Instituto de Investigaciones Biomédicas "Alberto Sols," Madrid, Spain) (50). Both constructs were cloned into the vector pcDNA5/FRT/TO (Invitrogen) to obtain the corresponding pcDNA5/FRT/TO-LOX and -BMP1 plasmids. These constructs were then co-transfected with the Flp recombinase expression plasmid pOG44 into the Flp-In T-REx 293 cell line using Lipofectamine 2000 (Invitrogen). These cells stably express the Tet repressor and contain a single integrated FRT (Flp recombination target) site. Flp recombi-

nase expression from the pOG44 vector mediates insertion of the cDNA cassettes into the genome at the integrated FRT site through site-specific DNA recombination. After 48 h, cells were selected for hygromycin B resistance (Roche Diagnostics, Barcelona, Spain), and clones appeared after 10–15 days. Isogenic pooled clones were expanded and checked for transgene expression after 48 h of incubation in the absence or presence of doxycycline (tetracycline analog) at 1 μg/ml. A construct for the overexpression of a fusion protein of human LOX and GFP (LOX–GFP) was generated by cloning of the LOX insert into pEGFP-N1 (Life Technologies, Inc.) and further transfer of the LOX–GFP chimera to pcDNA5/FRT/TO for expression in the Flp-In T-REx 293 system. Specific mutations in the tyrosine cluster of LOX or LOX–GFP proteins were introduced by site-directed mutagenesis using the primer CCTACAAGTACTCTGACGACAACCCT**TTCTTC**AAC**TTCTTC**GATACT**TTC**GAAAGGCCCAGACCTGGGGG (changed nucleotides shown in bold).

ADAMTS-overexpressing HEK293 cell clones were generated as described previously (15). Briefly, cells were transfected (Novagen GeneJuice® transfection reagent, EDM Millipore, Billerica, MA) with the pcDNA™ 6/TR expression vector (Invitrogen) and selected using blasticidin. Clones expressing a high level of the tetracycline repressor (TR) protein were identified by immunoblotting (rabbit polyclonal no. TET01, MoBiTec) and further transfected by the pcDNA4/TO expression vector (Tet-On System, Invitrogen) containing the complete coding sequence of ADAMTS2, ADAMTS3, or ADAMTS14 inserted in the "multiple cloning site" (NotI–XbaI sites for ADAMTS2 and ADAMTS14 and PmeI–PmeI sites for ADAMTS3). After selection (Zeocin, 300 μg/ml), subcloning was performed to identify clones producing ADAMTS2, ADAMTS3, or ADAMTS14 only in the presence of doxycycline. Semipurified preparations of ADAMTS enzymes were obtained as reported previously (51).

Protein analysis

To induce transgene expression in HEK293, cells were seeded on 100-mm culture dishes and incubated at 90% confluence with 5 ml of serum- and phenol red-free medium containing 1 μg/ml doxycycline (Dox) for 48 h. Cell supernatants were collected and concentrated down to about 200 μl using Amicon Ultracentrifugal filters (Ultracel-10K, EDM Millipore). Separately, cell monolayers were washed with PBS and lysed with 750 μl of Tris-SDS buffer (60 mM Tris-HCl, pH 6.8, 2% SDS) to obtain total-cell lysate. Protein concentration was determined by the BCA™ protein assay kit (Thermo Fisher Scientific, Rockford, IL). For analysis of LOX expression by standard one-dimensional (1D) electrophoresis coupled to immunoblotting, proteins were fractionated on SDS-polyacrylamide gels. Proteins were also analyzed by two-dimensional (2D) electrophoresis. For this type of studies, samples were precipitated with the methanol/chloroform method and then resuspended in lysis buffer (7 M urea, 2 M thiourea, 2% CHAPS, and 1% carrier ampholytes, pH 3–10 linear) and solubilized for 1 h at room temperature with agitation (52). Protein concentration was determined using Pierce™ 660-nm protein assay (Thermo Fisher Scientific). Protein extracts were diluted in rehydration buffer (7 M urea, 2 M thiourea, 2% CHAPS, 10 mM DTT, 1,2% DeStreak, and 1% carrier ampholytes, pH 3–11 nonlinear) up to a final volume of 200 μl and applied by active rehydration to 11-cm IPG strips, pH 3–11 NL (GE Healthcare). The first dimension was run at 75 μA/IPG strip in the IPGphor IEF System (GE Healthcare) following a voltage increase in eight steps. After the first dimension, strips were equilibrated with SDS equilibration buffer (50 mM Tris, pH 8.8, 6 M urea, 30% (v/v) glycerol, 2% (w/v) SDS, traces of bromphenol blue) containing 1% (w/v) DTT for 12 min and thereafter in the same buffer containing 4% (w/v) iodoacetamide for an additional 10 min. Then the proteins were separated on home-casted 12.5% Tris-glycine gels using an Mini Protean electrophoresis cell (Bio-Rad) at 25 °C until the tracking dye had migrated off the bottom of the gel. 1D and 2D gels were then transferred onto nitrocellulose membranes at 12 V for 20 min in a semi-dry Trans-Blot Turbo system (Bio-Rad). Membranes were blocked by incubation for 30 min with 1% BSA in Tris-buffered saline (TBS) containing 0.5% Tween 20, and antigens were detected using specific primary antibodies (LOX: ab31238, Abcam, Cambridge, UK; BMP1: AF1927, R&D Systems; anti-sulfotyrosine antibody: Sulfo-1C-A2, ab136481, Abcam; anti-GFP: catalog no. 11814460001, mouse monoclonal, Roche Diagnostics; ADAMTS2: homemade mouse mAb recognizing the fourth TSP1 repeat; ADAMTS3: 11-867-423-001, Roche Diagnostics, specific for human influenza hemagglutinin (HA)-tag inserted in the spacer domain; ADAMTS14: sc-67436, Santa Cruz Biotechnology, Dallas, TX). Blots were then developed and quantified using corresponding IRDye 680- or Li-Cor IRDye 800-labeled secondary antibodies with the Odyssey IR imaging system (Li-Cor).

LOX–GFP proteins were immunoprecipitated using GFP-Trap agarose beads (ChromoTek, Planegg-Martinsried, Germany) following the manufacturer's protocol. Immunoprecipitated proteins were analyzed as described above. For analysis of tyrosine sulfation, corresponding LOX–GFP-overexpressing HEK293 cell clones were plated on 100-mm culture dishes and grown until 90% confluence. Then, cells were rinsed three times with sulfate-free medium in which 0.8 mM $MgSO_4$ had been replaced with 0.8 mM $MgCl_2$. The dishes were then incubated for 48 h at 37 °C with sulfate-free medium containing 0.2 mCi of [^{32}S]sulfate (PerkinElmer Life Sciences) in the presence of 1 μg/ml Dox. After the incubation, the supernatants were collected and processed as described above for immunoprecipitation and electrophoresis analysis. Gels containing [^{32}S]sulfate-labeled proteins were soaked for 20 min in fixing solution (20% acetic acid, 10% methanol) and then dried and exposed to autoradiographic films (Agfa Healthcare, Mortsel, Belgium) or using a Fujifilm BAS-1500 phosphorimager (Fuji Photo Film Co. Ltd., Kanagawa, Japan).

Proteomic analysis

For analysis of the proteolytic processing site of LOX by ADAMTS2 enzyme, LOX supernatants were exposed to the protease for 4 h at 37 °C and then filtered through a 50-kDa cutoff Amicon ultracentrifugal filter (Ultracel-50K, Millipore) to enrich the sample in low-molecular weight polypeptides. Eluates were then applied onto 1.2-cm wide wells of a conven-

tional SDS-polyacrylamide gel (0.75-mm thick, 4% stacking, and 10% resolving). Electrophoresis was continued until the proteins became concentrated at the stacking/resolving gel interface. The unseparated protein bands were visualized by Coomassie staining, excised, cut into cubes (2 × 2 mm), and placed in 0.5-ml microcentrifuge tubes. The gel pieces were destained in acetonitrile/water (1:1), incubated with 10 mM DTT for 1 h at 56 °C for disulfide bond reduction and with 50 mM iodoacetamide for 1 h at room temperature in darkness for thiol group alkylation, and then digested *in situ* with sequencing grade trypsin (Promega, Madison, WI) as described previously (53). Digestion products were desalted onto OMIX Pipette C18 tips (Agilent Technologies) and analyzed by reverse phase-LC–tandem MS (RP-LC-MS/MS) in an Easy-nLC II system coupled to an ion trap linear trap quadrupole (LTQ)-Orbitrap-Velos-Pro hybrid mass spectrometer (Thermo Fisher Scientific). Peptide identification from raw data were carried out using PEAKS Studio 6 software (Bioinformatics Solutions Inc.) (54). Database search was performed against UniProt-*Homo sapiens*.fasta (decoy-fusion database). The following constraints were used for the searches: tryptic cleavage after Arg and Lys, up to two missed cleavage sites, allows nonspecific cleavage at one end of the peptide, and tolerances of 20 ppm for precursor ions and 0.6 Da for MS/MS fragment ions. The variable modifications allowed were methionine oxidation and cysteine carbamidomethylation. False discovery rate (FDR) was set as <1% (FDR < 0.01). Detected LOX sequences were screened for nontryptic internal peptides (no Lys or Arg in P1) as potential sites for ADAMTS processing.

To characterize the potential modification by tyrosine sulfation, LOX–GFP supernatants were exposed to BMP1 protease and immunoprecipitated with GFP-Trap agarose beads as described above. Afterward, immunoprecipitates were then fractioned by SDS-PAGE and analyzed by immunoblotting with anti-GFP antibody and stained for total protein with Coomassie Blue. Gel bands matching LOX–GFP precursor and processed forms were excised from the gel and manually digested with sequencing-grade AspN (Promega). For this digestion, gel plugs were alternatively washed several times with 25 mM ammonium bicarbonate and acetonitrile; thereafter, samples were reduced with 10 mM DTT for 1 h at 37 °C, followed by alkylation with 55 mM iodoacetamide for 30 min at room temperature before incubating with 0.1 μg of AspN for 18 h at 37 °C. Following digestion, peptides were extracted, pooled, dried by speed-vacuum centrifugation, and resuspended in 0.2% TFA in water for PRM analysis using an Eksigent 1D-nanoHPLC coupled to a 5600TripleTOF QTOF mass spectrometer (Sciex, Framingham, MA), equipped with a nano-ESI source and controlled by Analyst version 1.7 software (ABSciex). HPLC was equipped with a trap column Acclaim PepMap 100, 5-μm particle diameter, 100 Å pore size (Thermo Fisher Scientific), switched on-line with a silica-based reversed-phase column nanoACQUITY UPLC 75 μm × 15 cm, 1.7-μm particle size (Waters). The loading pump delivered a solution of 0.1% formic acid in 98% water, 2% acetonitrile (Scharlab, Barcelona, Spain) at 3 μl/min. The nanopump provided a flow rate of 250 nl/min and was operated under gradient elution conditions, using 0.1% formic acid in water as mobile phase A and 0.1% formic acid in 100% acetonitrile as mobile phase B. Gradient elution was performed according to the following scheme: isocratic conditions of 96% A and 4% B for 5 min, a linear increase to 40% B in 25 min, a linear increase to 95% B in 2 min, isocratic conditions of 95% B for 5 min, and return to initial conditions in 10 min. Injection volume was 5 μl.

The LC system was coupled via a nanospray source to the mass spectrometer. PRM analysis was conducted in negative ion mode with the ion spray voltage set at 2800 V. Initial PRM tests were also performed in positive ion mode. Drying gas temperature was set to 150 °C at a flow rate of 20 liters/min. Full scan MS spectra (m/z 230–1500) were acquired during 100 ms. Product ion scans of precursors with m/z values of 611.7, 651.8, and 691.8, corresponding to the unmodified, monosulfonated, and disulfonated variants of DDNPYYNYY ($M - 2H^+$), respectively, were acquired during 100 ms/cycle in the 100–1500 m/z range. Acquisition mode was of high-sensitivity, and both MS and MSMS spectra were analyzed using PeakView version 1.2 software (Sciex).

Sulfated synthetic DDNPYYNYY peptides were used to validate PRN analysis and to confirm the sequence identity. These peptides were synthesized in-house using standard Fmoc (*N*-(9-fluorenyl)methoxycarbonyl) chemistry in an Intavis Multiple peptide synthesizer (INTAVIS, Cologne, Germany).

Analysis of LOX enzymatic activity

LOX supernatants were assayed for enzymatic activity using the lysyl oxidase activity assay kit (Fluorometric) from Abcam. This assay is based on the widely used method described by Palamakumbura *et al.* (22) and uses a proprietary soluble LOX substrate in a horseradish peroxidase–coupled reaction with concomitant detection of hydrogen peroxide with Amplex Red reagent. Briefly, 50 μl of concentrated supernatant were mixed with an equivalent volume of reaction mixture in the presence or absence of 0.3 mM BAPN, a pan-inhibitor of lysyl oxidases. H_2O_2 release was measured every 3 min for a total period of 1 h at excitation and emission wavelengths of 525 and 580–640 nm, respectively, on a Glomax Multi Detection system (Promega). Enzyme activities were expressed as fluorescence arbitrary units and corrected for background levels determined in the presence of BAPN.

Solid-phase binding assay

Binding of the various LOX species to collagen was performed by a modification of the standard solid-phase binding assay (55). Telocollagen (RatCol, rat tail type I collagen solution) and atelocollagen (Nutragen, bovine type I collagen solution) (Advanced Biomatrix, San Diego) were coated overnight on Maxisorb 96-well-immunoplates (Nunc, Thermo Fisher Scientific) at 50 μg/ml in 16 mM acetic acid buffer and washed three times with HBS buffer (10 mM HEPES, 0.135 M NaCl, pH 7.4). Afterward, wells were blocked with 3% BSA in HBS buffer for 1 h and washed three times before the incubation with LOX-containing concentrated supernatants for 1 h at room temperature in HBS buffer containing 2 mM $CaCl_2$ and 15 μM $ZnSO_4$. Unbound proteins were extensively washed out with HBS buffer, and the remaining bound material was removed by addition of 30 ml of SDS-loading buffer and 5 min heating at 60 °C.

Unbound and bound fractions were then analyzed for LOX immunoreactivity by immunoblotting as described above. LOX proteins were quantified by densitometry, and the extent of binding was expressed as percentage of total.

Statistical analysis

Data are presented as the mean ± S.D. of n independent measurements as indicated in the corresponding figure legends. Statistical comparisons between groups were calculated by one-way ANOVA analysis followed by Bonferroni's post test for multiple-group comparisons using GraphPad Prism 6. The p values obtained are indicated in the figure legends when statistically significant ($p < 0.05$).

Protein alignments were performed with Clustal Omega at the European Bioinformatics Institute (EMBL-EBI) using sequences available in the NCBI (National Center for Biotechnology Information) protein database.

Author contributions—T. R.-G., A. P., G. B., L. D., M. B., and F. R.-P. investigation; T. R.-G., A. P., G. B., L. D., M. B., and F. R.-P. methodology; T. R.-G., A. C., and F. R.-P. writing-original draft; T. R.-G., A. P., M. B., A. C., and F. R.-P. writing-review and editing; A. C. and F. R.-P. conceptualization; A. C. and F. R.-P. formal analysis; A. C. and F. R.-P. supervision; A. C. and F. R.-P. funding acquisition; A. C. and F. R.-P. project administration; F. R.-P. data curation.

Acknowledgments—We thank Víctor L. Ruiz-Pérez (Instituto de Investigaciones Biomédicas "Alberto Sols," Madrid, Spain) for providing the plasmid pBabe-BMP1. Proteomic analysis was carried out at the CBMSO and CNB Protein Chemistry Facilities, which belong to the Spanish Proteomics Network ProteoRed, PRB3-ISCIII, supported by Grant PT17/0019.

References

1. Engel, J., and Chiquet, M. (2011) in *The Extracellular Matrix: an Overview* (Mecham, R. P., ed) pp. 1–39, Springer-Verlag, Berlin, Heidelberg
2. Kadler, K. E., Baldock, C., Bella, J., and Boot-Handford, R. P. (2007) Collagens at a glance. *J. Cell Sci.* **120,** 1955–1958 CrossRef Medline
3. Canty, E. G., and Kadler, K. E. (2005) Procollagen trafficking, processing and fibrillogenesis. *J. Cell Sci.* **118,** 1341–1353 CrossRef Medline
4. Eyre, D. R., and Wu, J. J. (2005) Collagen cross-links. *Top. Curr. Chem.* **247,** 207–229 CrossRef
5. Grau-Bové, X., Ruiz-Trillo, I., and Rodriguez-Pascual, F. (2015) Origin and evolution of lysyl oxidases. *Sci. Rep.* **5,** 10568 CrossRef Medline
6. Rodriguez-Pascual, F., and Slatter, D. A. (2016) Collagen cross-linking: insights on the evolution of metazoan extracellular matrix. *Sci. Rep.* **6,** 37374 CrossRef Medline
7. Trackman, P. C., Bedell-Hogan, D., Tang, J., and Kagan, H. M. (1992) Post-translational glycosylation and proteolytic processing of a lysyl oxidase precursor. *J. Biol. Chem.* **267,** 8666–8671 Medline
8. Uzel, M. I., Scott, I. C., Babakhanlou-Chase, H., Palamakumbura, A. H., Pappano, W. N., Hong, H. H., Greenspan, D. S., and Trackman, P. C. (2001) Multiple bone morphogenetic protein 1-related mammalian metalloproteinases process pro-lysyl oxidase at the correct physiological site and control lysyl oxidase activation in mouse embryo fibroblast cultures. *J. Biol. Chem.* **276,** 22537–22543 CrossRef Medline
9. Cronshaw, A. D., Fothergill-Gilmore, L. A., and Hulmes, D. J. (1995) The proteolytic processing site of the precursor of lysyl oxidase. *Biochem. J.* **306,** 279–284 CrossRef Medline
10. Panchenko, M. V., Stetler-Stevenson, W. G., Trubetskoy, O. V., Gacheru, S. N., and Kagan, H. M. (1996) Metalloproteinase activity secreted by fibrogenic cells in the processing of prolysyl oxidase: potential role of procollagen c-proteinase. *J. Biol. Chem.* **271,** 7113–7119 CrossRef Medline
11. Kagan, H. M., Sullivan, K. A., Olsson, T. A., 3rd., and Cronlund, A. L. (1979) Purification and properties of four species of lysyl oxidase from bovine aorta. *Biochem. J.* **177,** 203–214 CrossRef Medline
12. Vidal, G. P., Shieh, J. J., and Yasunobu, K. T. (1975) Immunological studies of bovine aorta lysyl oxidase: evidence for two forms of the enzyme. *Biochem. Biophys. Res. Commun.* **64,** 989–995 CrossRef Medline
13. Kuivaniemi, H. (1985) Partial characterization of lysyl oxidase from several human tissues. *Biochem. J.* **230,** 639–643 CrossRef Medline
14. Rosini, S., Pugh, N., Bonna, A. M., Hulmes, D. J. S., Farndale, R. W., and Adams, J. C. (2018) Thrombospondin-1 promotes matrix homeostasis by interacting with collagen and lysyl oxidase precursors and collagen cross-linking sites. *Sci. Signal.* **11,** eaar2566 CrossRef Medline
15. Bekhouche, M., Leduc, C., Dupont, L., Janssen, L., Delolme, F., Vadon-Le Goff, S., Smargiasso, N., Baiwir, D., Mazzucchelli, G., Zanella-Cleon, I., Dubail, J., De Pauw, E., Nusgens, B., Hulmes, D. J., Moali, C., and Colige, A. (2016) Determination of the substrate repertoire of ADAMTS2, 3, and 14 significantly broadens their functions and identifies extracellular matrix organization and TGF-β signaling as primary targets. *FASEB J.* **30,** 1741–1756 CrossRef Medline
16. Boak, A. M., Roy, R., Berk, J., Taylor, L., Polgar, P., Goldstein, R. H., and Kagan, H. M. (1994) Regulation of lysyl oxidase expression in lung fibroblasts by transforming growth factor-β1 and prostaglandin E2. *Am. J. Respir. Cell Mol. Biol.* **11,** 751–755 CrossRef Medline
17. Dupont, L., Ehx, G., Chantry, M., Monseur, C., Leduc, C., Janssen, L., Cataldo, D., Thiry, M., Jerome, C., Thomassin, J. M., Nusgens, B., Dubail, J., Baron, F., and Colige, A. (2018) Spontaneous atopic dermatitis due to immune dysregulation in mice lacking Adamts2 and 14. *Matrix Biol.* **70,** 140–157 CrossRef Medline
18. Kehoe, J. W., and Bertozzi, C. R. (2000) Tyrosine sulfation: a modulator of extracellular protein–protein interactions. *Chem. Biol.* **7,** R57–R61 CrossRef Medline
19. Yang, Y. S., Wang, C. C., Chen, B. H., Hou, Y. H., Hung, K. S., and Mao, Y. C. (2015) Tyrosine sulfation as a protein post-translational modification. *Molecules* **20,** 2138–2164 CrossRef Medline
20. Atsawasuwan, P., Mochida, Y., Katafuchi, M., Tokutomi, K., Mocanu, V., Parker, C. E., and Yamauchi, M. (2011) A novel proteolytic processing of prolysyl oxidase. *Connect. Tissue Res.* **52,** 479–486 CrossRef Medline
21. Monigatti, F., Gasteiger, E., Bairoch, A., and Jung, E. (2002) The sulfinator: predicting tyrosine sulfation sites in protein sequences. *Bioinformatics* **18,** 769–770 CrossRef Medline
22. Palamakumbura, A. H., and Trackman, P. C. (2002) A fluorometric assay for detection of lysyl oxidase enzyme activity in biological samples. *Anal. Biochem.* **300,** 245–251 CrossRef Medline
23. Trackman, P. C., and Kagan, H. M. (1979) Nonpeptidyl amine inhibitors are substrates of lysyl oxidase. *J. Biol. Chem.* **254,** 7831–7836 Medline
24. Kagan, H. M., Williams, M. A., Williamson, P. R., and Anderson, J. M. (1984) Influence of sequence and charge on the specificity of lysyl oxidase toward protein and synthetic peptide substrates. *J. Biol. Chem.* **259,** 11203–11207 Medline
25. Rodriguez-Pascual, F., and Rosell-Garcia, T. (2018) Lysyl oxidases: functions and disorders. *J. Glaucoma* **27,** S15–S19 CrossRef Medline
26. Blouin, S., Paschalis, E., Gupta, H., Fratzl-Zelman, N., Pischon, N., Trackman, P. C., Mäki, J. M., Roschger, P., and Klaushofer, K. (2010) Bone material properties in lysyl oxidase knock-out mice. *Bone* **47,** S80 CrossRef
27. Mäki, J. M., Räsänen, J., Tikkanen, H., Sormunen, R., Mäkikallio, K., Kivirikko, K. I., and Soininen, R. (2002) Inactivation of the lysyl oxidase gene Lox leads to aortic aneurysms, cardiovascular dysfunction, and perinatal death in mice. *Circulation* **106,** 2503–2509 CrossRef Medline
28. Mäki, J. M., Sormunen, R., Lippo, S., Kaarteenaho-Wiik, R., Soininen, R., and Myllyharju, J. (2005) Lysyl oxidase is essential for normal development and function of the respiratory system and for the integrity of elastic and collagen fibers in various tissues. *Am. J. Pathol.* **167,** 927–936 CrossRef Medline
29. Uzel, M. I., Shih, S. D., Gross, H., Kessler, E., Gerstenfeld, L. C., and Trackman, P. C. (2000) Molecular events that contribute to lysyl oxidase enzyme

activity and insoluble collagen accumulation in osteosarcoma cell clones. *J. Bone Miner. Res.* **15,** 1189–1197 CrossRef Medline
30. Cronlund, A. L., Smith, B. D., and Kagan, H. M. (1985) Binding of lysyl oxidase to fibrils of type I collagen. *Connect. Tissue Res.* **14,** 109–119 CrossRef Medline
31. Siegel, R. C. (1974) Biosynthesis of collagen crosslinks: increased activity of purified lysyl oxidase with reconstituted collagen fibrils. *Proc. Natl. Acad. Sci. U.S.A.* **71,** 4826–4830 CrossRef Medline
32. Kanan, Y., Siefert, J. C., Kinter, M., and Al-Ubaidi, M. R. (2014) Complement factor H, vitronectin, and opticin are tyrosine-sulfated proteins of the retinal pigment epithelium. *PLoS ONE* **9,** e105409 CrossRef Medline
33. Onnerfjord, P., Heathfield, T. F., and Heinegård, D. (2004) Identification of tyrosine sulfation in extracellular leucine-rich repeat proteins using mass spectrometry. *J. Biol. Chem.* **279,** 26–33 CrossRef Medline
34. Tillgren, V., Mörgelin, M., Önnerfjord, P., Kalamajski, S., and Aspberg, A. (2016) The tyrosine sulfate domain of fibromodulin binds collagen and enhances fibril formation. *J. Biol. Chem.* **291,** 23744–23755 CrossRef Medline
35. Kalamajski, S., Bihan, D., Bonna, A., Rubin, K., and Farndale, R. W. (2016) Fibromodulin interacts with collagen cross-linking sites and activates lysyl oxidase. *J. Biol. Chem.* **291,** 7951–7960 CrossRef Medline
36. Svensson, L., Aszódi, A., Reinholt, F. P., Fässler, R., Heinegård, D., and Oldberg, A. (1999) Fibromodulin-null mice have abnormal collagen fibrils, tissue organization, and altered lumican deposition in tendon. *J. Biol. Chem.* **274,** 9636–9647 CrossRef Medline
37. Kalamajski, S., Liu, C., Tillgren, V., Rubin, K., Oldberg, Å., Rai, J., Weis, M., and Eyre, D. R. (2014) Increased C-telopeptide cross-linking of tendon type I collagen in fibromodulin-deficient mice. *J. Biol. Chem.* **289,** 18873–18879 CrossRef Medline
38. Moali, C., and Hulmes, D. J. (2012) in *Extracellular Matrix: Pathobiology and Signaling* (Karamanos, N., ed) pp. 539–561, Walter de Gruyter, Berlin/Boston
39. Rawlings, N. D., Waller, M., Barrett, A. J., and Bateman, A. (2014) MEROPS: the database of proteolytic enzymes, their substrates and inhibitors. *Nucleic Acids Res.* **42,** D503–D509 CrossRef Medline
40. Marini, J. C., Forlino, A., Bächinger, H. P., Bishop, N. J., Byers, P. H., Paepe, A., Fassier, F., Fratzl-Zelman, N., Kozloff, K. M., Krakow, D., Montpetit, K., and Semler, O. (2017) Osteogenesis imperfecta. *Nat. Rev. Dis. Primers* **3,** 17052 CrossRef Medline
41. Colige, A., Sieron, A. L., Li, S. W., Schwarze, U., Petty, E., Wertelecki, W., Wilcox, W., Krakow, D., Cohn, D. H., Reardon, W., Byers, P. H., Lapière, C. M., Prockop, D. J., and Nusgens, B. V. (1999) Human Ehlers-Danlos syndrome type VII C and bovine dermatosparaxis are caused by mutations in the procollagen I *N*-proteinase gene. *Am. J. Hum. Genet.* **65,** 308–317 CrossRef Medline
42. Bekhouche, M., and Colige, A. (2015) The procollagen N-proteinases ADAMTS2, 3 and 14 in pathophysiology. *Matrix Biol.* **44–46**, 46–53
43. Le Goff, C., Somerville, R. P., Kesteloot, F., Powell, K., Birk, D. E., Colige, A. C., and Apte, S. S. (2006) Regulation of procollagen amino-propeptide processing during mouse embryogenesis by specialization of homologous ADAMTS proteases: insights on collagen biosynthesis and dermatosparaxis. *Development* **133,** 1587–1596 CrossRef Medline
44. Guo, D.-C., Regalado, E. S., Gong, L., Duan, X., Santos-Cortez, R. L. P., Arnaud, P., Ren, Z., Cai, B., Hostetler, E. M., Moran, R., Liang, D., Estrera, A., Safi, H. J., University of Washington Center for Mendelian Genomics, Leal, S. M., *et al.* (2016) LOX mutations predispose to thoracic aortic aneurysms and dissections. *Circ. Res.* **118,** 928–934 CrossRef Medline
45. Lee, V. S., Halabi, C. M., Hoffman, E. P., Carmichael, N., Leshchiner, I., Lian, C. G., Bierhals, A. J., Vuzman, D., Brigham Genomic Medicine, Mecham, R. P., Frank, N. Y., and Stitziel, N. O. (2016) Loss of function mutation in LOX causes thoracic aortic aneurysm and dissection in humans. *Proc. Natl. Acad. Sci. U.S.A.* **113,** 8759–8764 CrossRef Medline
46. Hunt, S. E., McLaren, W., Gil, L., Thormann, A., Schuilenburg, H., Sheppard, D., Parton, A., Armean, I. M., Trevanion, S. J., Flicek, P., and Cunningham, F. (2018) Ensembl variation resources. *Database* **2018** CrossRef
47. Busnadiego, O., González-Santamaría, J., Lagares, D., Guinea-Viniegra, J., Pichol-Thievend, C., Muller, L., and Rodríguez-Pascual, F. (2013) LOXL4 is induced by transforming growth factor β1 through Smad and JunB/Fra2 and contributes to vascular matrix remodeling. *Mol. Cell. Biol.* **33,** 2388–2401 CrossRef Medline
48. Puig, M., Lugo, R., Gabasa, M., Giménez, A., Velásquez, A., Galgoczy, R., Ramírez, J., Gómez-Caro, A., Busnadiego, Ó., Rodríguez-Pascual, F., Gascón, P., Reguart, N., and Alcaraz, J. (2015) Matrix stiffening and β1 integrin drive subtype-specific fibroblast accumulation in lung cancer. *Mol. Cancer Res.* **13,** 161–173 CrossRef Medline
49. Rodríguez-Pascual, F., Redondo-Horcajo, M., and Lamas, S. (2003) Functional cooperation between Smad proteins and activator protein-1 regulates transforming growth factor-β-mediated induction of endothelin-1 expression. *Circ. Res.* **92,** 1288–1295 CrossRef Medline
50. Martínez-Glez, V., Valencia, M., Caparrós-Martín, J. A., Aglan, M., Temtamy, S., Tenorio, J., Pulido, V., Lindert, U., Rohrbach, M., Eyre, D., Giunta, C., Lapunzina, P., and Ruiz-Perez, V. L. (2012) Identification of a mutation causing deficient BMP1/mTLD proteolytic activity in autosomal recessive osteogenesis imperfecta. *Hum. Mutat.* **33,** 343–350 CrossRef Medline
51. Colige, A., Ruggiero, F., Vandenberghe, I., Dubail, J., Kesteloot, F., Van Beeumen, J., Beschin, A., Brys, L., Lapière, C. M., and Nusgens, B. (2005) Domains and maturation processes that regulate the activity of ADAMTS-2, a metalloproteinase cleaving the aminopropeptide of fibrillar procollagens types I–III and V. *J. Biol. Chem.* **280,** 34397–34408 CrossRef Medline
52. Wessel, D., and Flügge, U. I. (1984) A method for the quantitative recovery of protein in dilute solution in the presence of detergents and lipids. *Anal. Biochem.* **138,** 141–143 CrossRef Medline
53. Shevchenko, A., Wilm, M., Vorm, O., and Mann, M. (1996) Mass spectrometric sequencing of proteins silver-stained polyacrylamide gels. *Anal. Chem.* **68,** 850–858 CrossRef Medline
54. Zhang, J., Xin, L., Shan, B., Chen, W., Xie, M., Yuen, D., Zhang, W., Zhang, Z., Lajoie, G. A., and Ma, B. (2012) PEAKS DB: *de novo* sequencing assisted database search for sensitive and accurate peptide identification. *Mol. Cell. Proteomics* **11,** M111.010587 CrossRef Medline
55. Mould, P. A. (2009) Solid phase assays for studying ECM protein-protein interactions. *Methods Mol. Biol.* **522,** 195–200 CrossRef Medline

Differential cleavage of lysyl oxidase by the metalloproteinases BMP1 and ADAMTS2/14 regulates collagen binding through a tyrosine sulfate domain

Tamara Rosell-García, Alberto Paradela, Gema Bravo, Laura Dupont, Mourad Bekhouche, Alain Colige and Fernando Rodriguez-Pascual

J. Biol. Chem. 2019, 294:11087-11100.
doi: 10.1074/jbc.RA119.007806 originally published online May 31, 2019